Available online at www.sciencedirect.com
SCIENCE DIRECT
International Journal of Heat and Mass Transfer 49 (2006) 2523–2534
International Journal of HEAT and MASS TRANSFER
www.elsevier.com/locate/ijhmt

Experimental and theoretical investigation of film condensation with noncondensable gas

Seungmin Oh [1], Shripad T. Revankar *

School of Nuclear Engineering, Purdue University West Lafayette, IN 47907, USA

Received 30 June 2005; received in revised form 6 October 2005
Available online 20 March 2006

Abstract

Experimental and theoretical investigations were conducted for the film condensation with noncondensable gas in a vertical tube. Condensation experiments were performed for a steam–air mixture in a vertical tube submerged in a water pool where the heat from the condenser tube was removed through a boiling heat transfer. Degradation of the condensation with noncondensable gas was investigated. A heat and mass analogy model for the annular filmwise condensation with noncondensable gas was developed. In the steam–air mixture region, general momentum, heat and mass transport relations derived by analytic method were used with the consideration of surface suction effect. The predictions from the model were compared with the experimental data and the agreement was satisfactory.

Keywords: Film condensation; Noncondensable gas; Heat and mass analogy model; Blowing parameter

1. Introduction

The heat transfer analysis of film condensation is an important area in the design of heat exchangers. The condensation phenomenon plays an important role in the heat transfer process of the chemical and power industry, including nuclear power plants. This mode of heat transfer is often used because high heat transfer coefficients can be achieved. However, in practical operations of the condensers, small amounts of noncondensable (NC) gas may exist in working vapors due to characteristics of the system. It is well known that the presence of NC gas in a vapor can greatly reduce the performance of the condensers [1]. The NC gas is carried with vapor toward the interface where NC gas accumulates and vapor condenses. The NC gas boundary layer is developed as condensation proceeds along the condenser tube. This NC gas boundary layer serves as a resistance for the steam condensation.

In the General Electric's simplified boiling water reactor (SBWR), the passive containment cooling system (PCCS) was designed to remove the reactor core decay heat to the outside of the containment via steam condensation after a postulated loss of coolant accident [2]. The relevant separate effects experiments on the PCCS condenser under the presence of NC gas were conducted by Vierow [3], Siddique [4], Kuhn [5], and Park and No [6] with the secondary jacket cooling method. These tests provided a database and correlation for forced convection condensation of steam in a vertical tube in the presence of NC gas. These experiments used secondary jacket to remove heat from the condenser tube, where highly subcooled water supplied at the bottom of the jacket is heated along the condenser tube, and exits from the top of the jacket. However, actual PCCS condenser tubes are submerged in a water pool. During a postulated accident, the secondary pool quickly reaches at the saturated condition. So, the boundary condition at the actual PCCS condenser is a constant water temperature and heat transfer

* Corresponding author. Tel.: +1 765 496 1782; fax: +1 765 494 9570.
E-mail addresses: soh@ecn.purdue.edu (S. Oh), shripad@ecn.purdue.edu (S.T. Revankar).
[1] Tel.: +1 765 496 3906.

0017-9310/$ - see front matter © 2006 Elsevier Ltd. All rights reserved.
doi:10.1016/j.ijheatmasstransfer.2006.01.021

Nomenclature

A	heat transfer area
b_f	blowing parameter for momentum transfer
b_h	blowing parameter for heat transfer
b_m	blowing parameter for mass transfer
C_p	specific heat
d	diameter
f	friction coefficient
g	gravitational constant
g_m	mass transfer conductance
G	mass flux
h	heat transfer coefficient (HTC)
h_{fg}	latent heat of vaporization
j	diffusion mass flux
k	thermal conductivity
L	length
L^*	characteristic length scale $= \left(\mu_L^2/\rho_L(\rho_L-\rho)g\right)^{1/3}$
M	molecular weight
m	mass flow rate
m''	mass flux
Nu	Nusselt number
p	pressure
Pr	Prandtl number
Q	heat transfer rate
q	heat flux
r	radial coordinate
Re	Reynolds number
Sc	Schmidt number
Sh	mass transfer Sherwood number $= g_m d/(\rho D)$
St	heat transfer Stanton number $= Nu/(Re\,Pr)$
St_m	mass transfer Stanton number $= Sh/(Re\,Sc)$
T	temperature
u	axial velocity
v	radial velocity
W	noncondensable gas mass fraction
y	wall coordinate
z	axial or streamwise coordinate

Greek symbols

Γ	mass flow rate per unit length
δ	film thickness
δ^*	dimensionless film thickness $= \delta/L^*$
μ	dynamic viscosity
ν	kinematic viscosity
ρ	density
τ	shear stress
τ_I^*	dimensionless interfacial shear $= \tau_I/(\rho_L-\rho)gL^*$

Subscripts

avg	average
b	bulk
c	condensation
cond	gas region condensation
G	vapor–gas mixture
g	gas
I	interface
i	inside
in	inlet
L	liquid
lam	laminar
R	ratio
SAT	saturation
sen	sensible
TOT	total
tur	turbulent
v	vapor
W	wall
∞	free stream
0	quantity at no transpiration

mechanism at the secondary side is the boiling heat transfer. But for the secondary cooling jacket method the boundary condition has a varying coolant temperature with forced convective heat transfer. Therefore, a new database is needed on the in-tube steam condensation submerged in a water pool.

The theoretical analysis of the condensation from a vapor–gas mixture in a tube has been studied by many researchers. The analysis of the heat and mass transfer during condensation of a vapor in the presence of NC gas has generally involved either the boundary layer method or the heat and mass analogy method. Since Colburn and Hougen's work [7], there have been many researches on the heat and mass analogy method [8–14]. This method generally calculates the condensation mass transfer rate from the analogy of heat and mass transfer. Also, interfacial friction factor or interfacial shear stress is calculated based on the single phase correlations and two phase empirical or semi-empirical correlations. Although simplicity in this method is a good advantage, a careful attention should be paid to the choice of the momentum, heat and mass transport correlations.

For the systematic understanding of the transport phenomena of the momentum, heat and mass, the boundary layer method, which is solving the governing equations with a boundary layer approximation in the gas-mixture and liquid film regions, has been studied. Recently, authors [15] performed the filmwise condensation analysis using the boundary layer method. Based on this boundary layer analysis, the transport quantities, such as interfacial friction factor, heat transfer Nusselt number and mass transfer Sherwood number, are calculated and these are compared with various correlations in literature. From the comparison, appropriate correlations for each transport quantity are selected and the heat and mass analogy model is developed based on the correlations.

2. Condensation experiment

Condensation experiment is performed to investigate the effects of noncondensable gas in a vertical tube condenser. A scale-down condenser tube from the prototypic SBWR PCCS condenser is fabricated and submerged in a water pool, so the secondary heat removal mechanism of the condenser is boiling heat transfer.

2.1. Experimental facility

The test loop is comprised of steam generator, instrumented condenser test section with secondary pool boiling section, condensate tank, suppression pool, water storage tank, air supply line, and associated piping and instrumentation. The schematic diagram of the test loop and test section is shown in Fig. 1. A half-length and half-diameter scaling was used in the present design. Important scaling parameters are shown in Table 1. An immersion type sheathed electrical heater of 10 kW capacity is mounted at the lower flange of the steam generator (SG).

For the pool boiling heat removal at the secondary side, test section is designed with two subassemblies, primary condensing tube and secondary boiling tube. The primary condensing tube is made of 26.6 mm inside diameter, 3.38 mm thickness, 2.4 m long Type 304 stainless steel pipe with insulation housing (108 mm ID, 114 mm OD). The secondary boiling tube is made of Type 304 stainless steel pipe with 161 mm ID. Active tube length of condensation is 0.984 m. To separate the active condenser region from upstream pipe, the insulation housing is welded at the top of the active condenser with a 6.35 mm thick plate. This thickness of 6.35 mm plate is included in the active tube length. The gap between the primary condensing tube and the insulation housing is filled with the fiberglass thermal insulation material to minimize the conduction heat transfer above the active condenser.

The condensation can occur before the inlet of active condenser due to the heat conduction through the tube wall. The effect of the heat conduction in the inlet region was investigated with the numerical analysis by solving the steady state heat conduction equation for the primary condensing tube and the insulation housing [16]. The extended condensation length where the condensation initiates before the inlet of the active condenser was estimated to be less than 1.5% of the active length for the present test conditions. Therefore, the effect of the heat conduction is not accounted for the data reduction.

The annulus between the primary condensing tube and the secondary boiling tube is filled with water and serves as a water pool. The secondary pool is maintained at saturation condition during experiment. At different axial and circumferential location of the active tube, five nozzles are welded for inside bulk temperature measurement. At the opposite side of each nozzle, a thermocouple junction is made to measure the tube outside wall temperature. To measure the secondary side temperature, six thermocouples are installed at the secondary pool at different axial locations. The measured secondary pool temperature at the active condenser section was around 101.5–103 °C. These temperatures correspond to the saturation temperature at the secondary pool pressure considering the hydrostatic head. The evaporation rate during the experiment is calculated by the level measurement of the secondary pool. By use of the insulation housing, the pool cross-sectional area of the steam rising section is reduced. It gives a magnified water level difference due to evaporation. Hence, it provides more accurate measurement of evaporation rate.

A steady state steam flow rate is obtained with the SG pressurized to 1.15 MPa. This pressure is maintained during the experiment. Since the condensation experiments are performed below 0.5 MPa at the test section, the steam flow is choked at the flow control valve located at downstream of the SG. So, steam mass flow rate is independent of the pressure condition at the test section. For a given test section pressure, various steam mass flow rates can be obtained by regulating the flow control valve. Also for a given steam mass flow rate, various test pressure conditions can be established by setting the suppression pool pressure. When the SG pressure reach to about 1.15 MPa, the flow control valve is opened and steam condensation begins in the test section that heats up the secondary water pool. When the saturation condition is achieved at the secondary pool and NC gas flow rate is stabilized, the data is acquired.

More details for the experimental facility, test procedure and data reduction method are reported in the authors' previous paper [17].

2.2. Test results

Condensation experiments were conducted with inlet steam flow rate 2.5–5.5 g/s, system pressure 0.12–0.4 MPa, inlet NC gas mass fraction 0–10%. The measurement errors associated with the average condensation HTC and condensation heat transfer rate were analyzed using the standard error propagation method. The mean error of condensation heat transfer rate was 1.5%. The condensation HTC is largely affected by the system pressure. Temperature difference, which is the driving force for condensation heat transfer, decreases as system pressure decreases. Since the temperature difference term is located at the denominator in Eq. (11), the error increases as the temperature difference decreases or system pressure decreases. The error of the average condensation HTC is around 30% when system pressure is 180 kPa and it is less than 10% when system pressure is greater than 300 kPa. Theoretically, the error can be an infinite value as system pressure approaches to its secondary pressure, i.e., the temperature difference between the primary saturation temperature and inside wall temperature approaches to zero. Mean error for all the data is 11%. A detailed description for the error analysis is presented in [16].

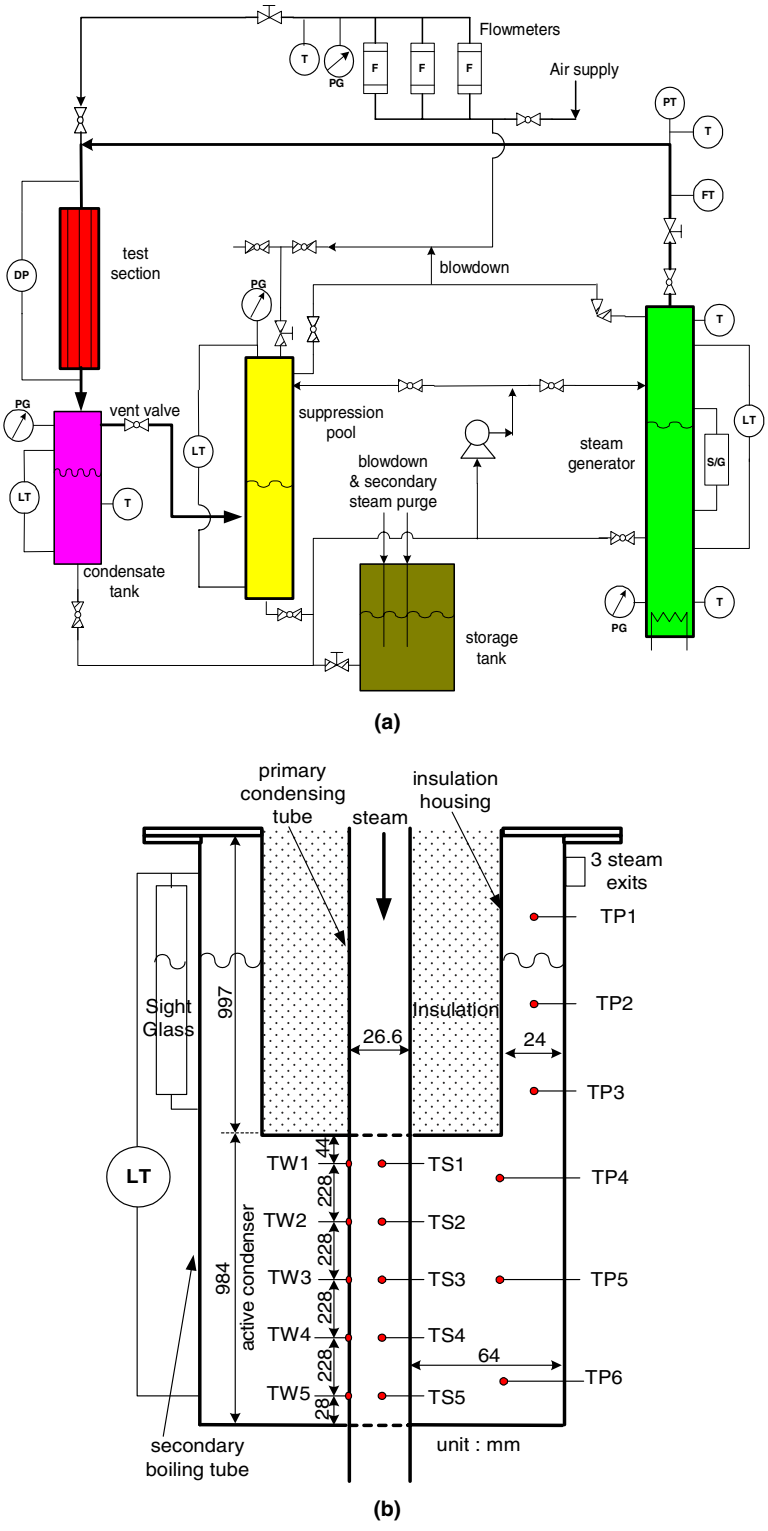

Fig. 1. Schematic diagram of experimental loop: (a) test loop and (b) test section.

Fig. 2 shows the effect of the inlet NC gas mass fraction. The condensation heat transfer rate and the condensation HTC decreases as inlet NC gas mass fraction increases. Since the NC gas is impermeable to the liquid film, it is accumulated at the film–gas interface so its concentration is very high. This high NC gas concentration region is propagating to the gas core region by mass diffusion. So the boundary layer thickness is getting thicker and the concentration level is increasing along the condenser tube length. Steam in the gas core region must diffuse long

Table 1
Single tube scaling parameters

Parameters	Prototype	Model	Model to prototype ratio
Length (m)	1.8	0.984	$L_R = 0.547$
Diameter (mm)	47.5	26.6	$d_R = 0.56$
Length to diameter ratio	37.9	37.0	$(L/d)_R = 0.976$
Heat transfer area (m^2)	0.2686	0.0822	$A_R = 0.306$
Average condensation HTC ratio for pure steam	–	–	$(h_{c,avg})_R = (L_R)^{-0.25} = 1.163$
Design heat removal capacity (kW)	20.16	7.18	$(h_{c,avg})_R \cdot A_R = 0.357$

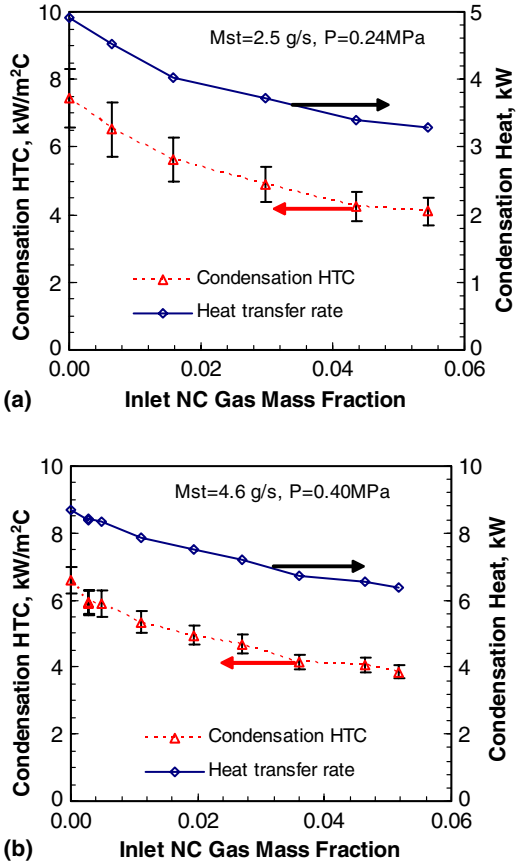

Fig. 2. Effect of inlet NC gas mass fraction.

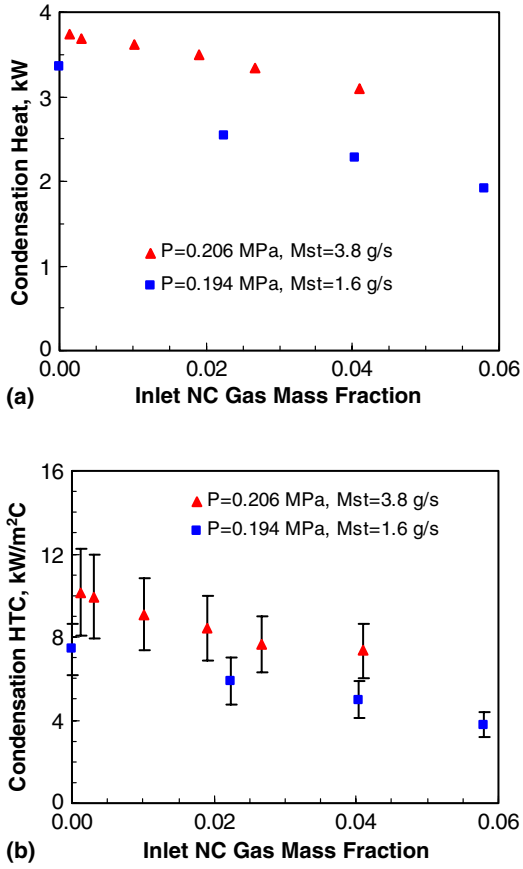

Fig. 3. Effect of inlet steam flow rate: (a) condensation heat transfer rate and (b) condensation heat transfer coefficient.

distance in high NC gas concentration boundary layer to condense at the interface. The developing NC gas boundary layer acts as a strong resistance to the condensation. The error bar of the condensation HTC data drawn in the figure shows the pressure dependency. For the low pressure condition of 0.24 MPa in Fig. 2(a), the relative error is 9.9–12.2%. However, it is 5.1–6.5% for high pressure condition of 0.40 MPa in Fig. 2(b). Since the error of the condensation heat transfer rate is very small (mean error of 1.5%), the error bar is not drawn in the figure.

The effect of inlet steam flow rate on the condensation HTC is shown in Fig. 3. Two different sets of inlet steam flow conditions at nominal system pressure of 0.2 MPa are plotted with inlet NC gas mass fraction. Condensation HTC decreases with NC gas mass fraction for a given steam flow condition. Higher steam flow results in higher condensation HTC. As inlet steam flow rate increases, interfacial shear also increases. This results in thinner liquid film, i.e., smaller resistance in heat transfer. Higher interfacial shear also enhance the heat transfer by early transition from laminar to turbulent flow in film region and by promoting the interface waves and ripples.

The effect of the system pressure is presented in Fig. 4 at the inlet steam flow rate of 3.6 g/s. Condensation heat transfer rate and condensation HTC for two sets of system pressure, 0.28 and 0.32 MPa, are plotted with inlet NC gas mass fraction. For a given pressure condition, the condensation heat removal rate and condensation HTC decrease with an increase in the NC gas mass fraction. As system

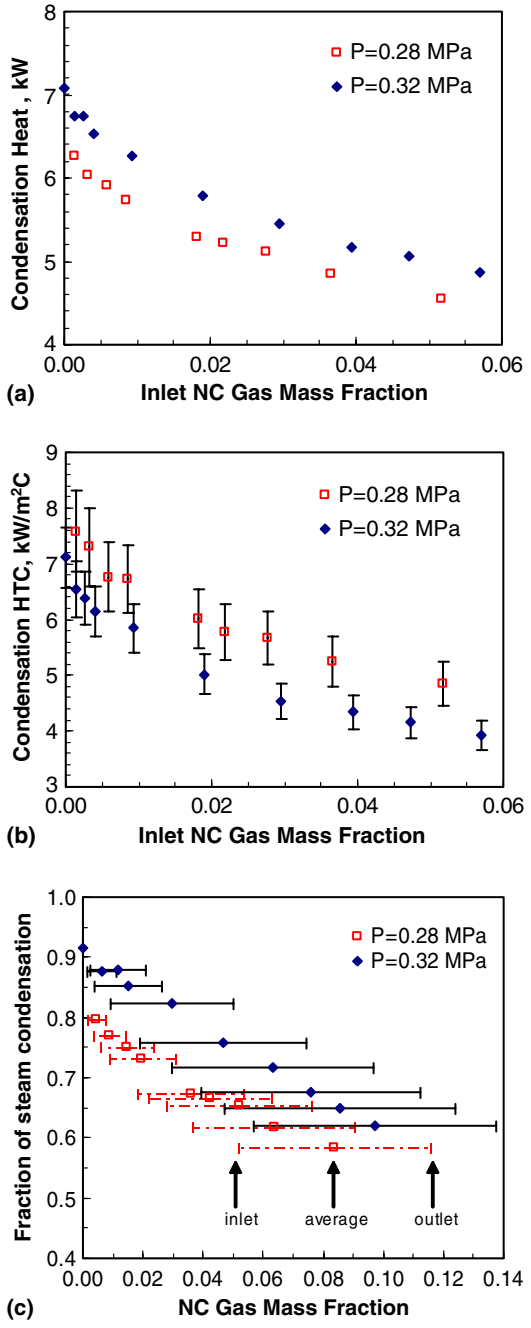

Fig. 4. Effect of pressure at inlet steam flow rate = 3.6 g/s: (a) condensation heat transfer rate, (b) condensation heat transfer coefficient and (c) fraction of stream condensed.

pressure increases, the condensation heat transfer rate also increases. However, the condensation HTC decreases with system pressure. These results are consistent with the theoretical Nusselt solution where the condensation HTC decreases with the temperature difference between inside wall and steam saturation temperature. As system pressure increases, the temperature difference increases more rapidly than the increase of condensation heat removal rate. Large temperature difference enhances the condensation rate, which results in thicker liquid film. Since the liquid film acts as a resistance for the heat transfer, the condensation HTC decreases as system pressure increases.

Until now, the condensation data are plotted with inlet NC gas mass fraction. For a given inlet NC gas fraction, the amount of steam condensed is a function of system pressure and inlet flow conditions. Therefore, tube average (or outlet) NC gas fraction is not equal for the same inlet NC gas fraction conditions. For the purpose of the up-scale of the present data to the prototype condition, the data presentation with inlet NC gas fraction is more useful. However, the amount of the steam condensed and the range of the NC gas fraction provide additional information. Fig. 4(c) shows the fraction of steam condensed (=condensation rate/inlet steam flow rate) with tube average NC gas mass fraction. *X*-axis bar in the plot shows the inlet and outlet NC gas mass fraction for each case. As expected, the higher fraction of condensation is achieved for the lower inlet (or average) NC gas mass fraction. The wider range of the NC gas fraction is shown for the higher inlet NC gas fraction. Also, it shows that more steam is condensed for the higher system pressure condition for the same inlet steam flow rate of 3.6 g/s.

2.3. Applicability of data to prototype

Data obtained from present half-length and half-diameter scale test facility should be properly up-scaled to be used in prototype condition. Important scaling parameters based on single condenser tube are summarized in Table 1.

The change in tube diameter has relatively small effects on the condensation heat transfer as long as the tube diameter is large enough compared with the liquid film thickness. However, the length of condenser tube can explicitly affects the condensation heat transfer. From the theoretical Nusselt solution for pure steam condensation, the local and average condensation HTC varies with $-1/4$ power of the tube length [1]. Therefore, the average condensation HTC for short length model tube will be greater than that for prototype condenser tube with the ratio of

$$(h_{c,avg})_R = \frac{(h_{c,avg})_{Model}}{(h_{c,avg})_{Prototype}} = (L_R)^{-0.25} = 1.163. \quad (1)$$

By assuming same fluid properties and pressure condition, the following can be obtained:

$$dT_R = (h_{fg})_R = \rho_R = \mu_R = k_R = 1. \quad (2)$$

Then, the ratio of heat flux or condensation mass flux is equal to the ratio of the average HTC:

$$(q)_R = (m''_c)_R = (h_{c,avg})_R = 1.163. \quad (3)$$

Heat transfer rate or condensation rate ratio can be obtained as

$$(Q)_R = (m_c)_R = (q)_R \cdot A_R = 0.357. \quad (4)$$

To validate these relationships, the pure steam cases are analyzed for the model and prototype geometry with the analogy model developed in next section. For the analysis of prototype condition, the inlet flow rate should be properly up-scaled. The ratio of inlet flow rate can be selected as the ratio of condensation rate in Eq. (4):

$$(m_{G,in})_R = (m_c)_R = 0.357. \quad (5)$$

Then, the ratio of inlet Reynolds number can be calculated as follows:

$$(Re_{in})_R = \left(\frac{\rho_G \cdot u_{G,in} \cdot d}{\mu_G}\right)_R = \left(\frac{4 \cdot m_{G,in}}{\pi \cdot d \cdot \mu_G}\right)_R = \left(\frac{m_{G,in}}{d}\right)_R = 0.638. \quad (6)$$

Fig. 5(a) shows the model to prototype ratio of the average condensation HTC, $(h_{c,avg})_R$, for pure steam cases predicted by the analogy model. The predicted ratios are very close to the theoretical value of 1.163 as given in Eq. (1). For the NC gas cases, the same analysis for the model and prototype geometry is performed with inlet Reynolds number ratio in Eq. (6). The model experiment conditions are inlet steam flow rate of 3.8 g/s and system pressure of 0.27 MPa. As shown in Fig. 5(b), the condensation HTC ratios for the NC gas condition are slightly greater than the theoretical value of 1.163 from pure steam Nusselt solution in Eq. (1). It means that the condensation performance of the prototype tube for NC gas condition is more degraded than that for pure steam condition. This is due to the additional heat transfer resistance, the NC gas boundary layer region, for the NC gas cases. For the pure steam cases, the condensation for longer tube is degraded only due to the increasing film thickness. For the NC gas cases, the condensation is further degraded due to the development of the NC gas boundary layer as the tube length increases. It is also notable from the Fig. 5(b) that the degradation is larger as inlet NC gas mass fraction increases. Therefore, short condenser tube is more efficient as far as the heat removal capacity is concerned.

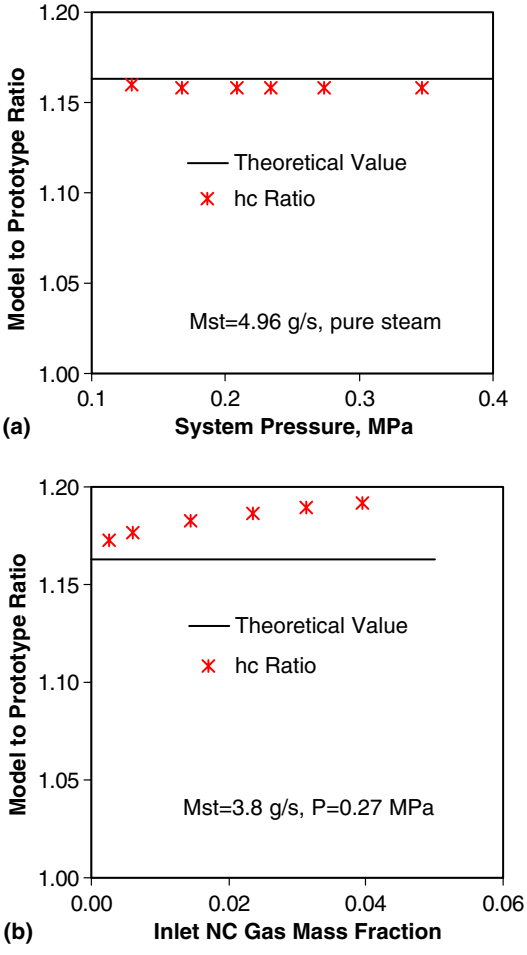

Fig. 5. Model to prototype ratio of condensation HTC predicted by analogy model: (a) pure steam cases and (b) NC gas cases.

It is worthy to discuss the effects of the entrance length. As condensation proceeds along the tube, the NC gas boundary layer is developing. From the boundary layer analysis for air-steam system [16], it was found that the boundary layer for velocity, temperature, and NC gas mass fraction is almost fully developed around $L/d = 15$ for different diameters. This region $(0 < L/d < 15)$ can be regarded as an entrance length in a sense of the NC gas boundary layer. However, this region is not necessarily a true entrance region as an aspect of the condensation HTC. Condensation is characterized by a very high condensation HTC at the inlet. So, the developing boundary layer region will not have considerable effects on the condensation, especially for pure steam or low inlet NC gas conditions. Even for a very high NC gas condition, the present scaling method will be valid since L/d for model and prototype is 37.0 and 37.9, respectively. As a general guideline, the applicable range of the present scaling method can be set as $L/d > 15$.

3. Heat and mass analogy model

The heat and mass analogy method is based on the heat balance at the liquid-gas interface, where the heat transferred from the vapor–gas boundary layer is equated to the heat transferred through the condensate film. The heat transfer from the gas region is the sum of the sensible cooling of bulk mixture and latent heat of condensation. To balance the heat transfer rate between film and mixture regions, the interface temperature is determined iteratively. These procedures are repeated along the condenser length.

3.1. Energy balance

The physical model of the film condensation in a tube is shown in Fig. 6. Variables or properties related with liquid film, vapor, and NC gas are respectively denoted with subscript L, v, and g. However, those related with vapor–gas mixture have no subscript for simplicity in the presentation of equations. The vapor–gas mixture is assumed to be saturated for the present model. Heat transfer in the

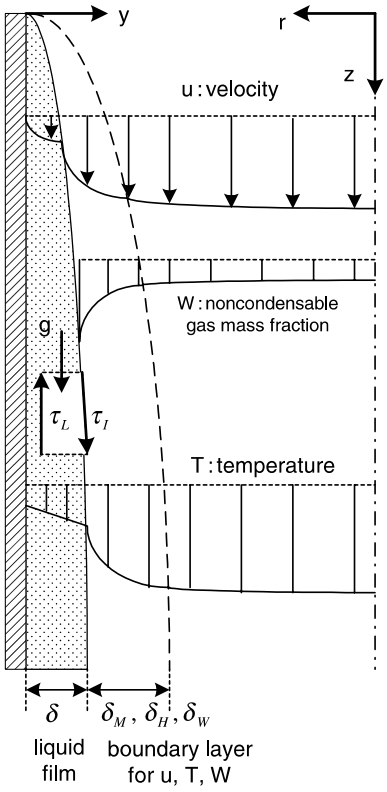

Fig. 6. Physical model for film condensation.

gas–vapor mixture region consists of the latent heat of condensation and sensible heat transfer. Then heat flux at the mixture-liquid film interface can be written as

$$q_{TOT} = q_{cond} + q_{sen} = m''_c \cdot h_{fg} + h_{sen} \cdot (T_{SAT} - T_I). \quad (7)$$

All the flux terms in this analysis such as heat flux, mass flux, and diffusion flux are based on the tube inside surface area. The gas region heat transfer rate must be balanced with heat transfer rate at film region, i.e.,

$$q_{TOT} = q_L = h_L \cdot (T_I - T_{Wi}). \quad (8)$$

From the latent heat of condensation and the temperature difference between interface and bulk saturation, a condensation HTC (h_{cond}) can be defined as

$$h_{cond} \equiv \frac{m''_c \cdot h_{fg}}{(T_{SAT} - T_I)}. \quad (9)$$

By substituting Eq. (9) into (7) and equating to Eq. (8),

$$h_L \cdot (T_I - T_{Wi}) = (h_{cond} + h_{sen}) \cdot (T_{SAT} - T_I). \quad (10)$$

Total condensation HTC for the annular film condensation can be defined as

$$h_c \equiv \frac{q_{TOT}}{(T_{SAT} - T_{Wi})}. \quad (11)$$

It should be noted that h_{cond} is the HTC defined as Eq. (9) which takes account of the condensation heat transfer in gas region only. However, h_c is total condensation HTC defined as Eq. (11) which reflects the heat transfer resistance of film, gas region condensation, and gas region sensible heat transfer. To avoid the confusion between these two condensation HTC, h_{cond} is called as gas region condensation HTC, hereafter.

Total resistance of heat transfer which is an inverse of total condensation HTC can be expressed as sum of individual resistance:

$$\frac{1}{h_c} = \frac{1}{h_L} + \frac{1}{h_{cond} + h_{sen}}. \quad (12)$$

To obtain h_c, the heat transfer components (h_L, h_{cond} and h_{sen}) should be estimated and the procedures to calculate these components are presented in the following sections.

3.2. Liquid film model

For the liquid film, the force balance in the control volume in Fig. 6 can be described as

$$\tau_L = (\rho_L - \rho) \cdot g \cdot (\delta - y) + \tau_I. \quad (13)$$

Liquid film is assumed to be laminar for the film thickness calculation. For laminar film, the velocity profile in the liquid film can be obtained from the above equation:

$$u_L(y) = \frac{(\rho_L - \rho) \cdot g}{\mu_L}\left(\delta \cdot y - \frac{y^2}{2}\right) + \frac{\tau_I}{\mu_L} y. \quad (14)$$

The first term in the right hand side of above equation is the parabolic velocity distribution, which is exactly same with Nusselt analysis for no interfacial shear. The second term is the linear velocity distribution due to the interfacial shear. The liquid film mass flow rate (m_L) can be calculated by integrating the velocity profile. Then, mass balance in liquid film can be expressed with respect to the film thickness as follows:

$$\Gamma \equiv \frac{m_L}{\pi \cdot d} = \frac{(\rho_L - \rho) \cdot g}{3\nu_L}\delta^3 + \frac{\tau_I}{2\nu_L}\delta^2. \quad (15)$$

Above equation can be simplified by use of dimensionless parameter as

$$Re_L \equiv \frac{4\Gamma}{\mu_L} = \frac{4}{3}(\delta^*)^3 + 2 \cdot \tau_I^* \cdot (\delta^*)^2. \quad (16)$$

By solving Eq. (16), film thickness can be calculated. If there is no interfacial shear, the Nusselt film thickness [1] can be explicitly obtained.

For laminar film, the temperature distribution in the film region is almost linear. Therefore film heat transfer coefficient can be written as

$$h_L = \frac{k_L}{\delta}. \quad (17)$$

Film Nusselt number is defined as follow:

$$Nu_L \equiv \frac{h_L \cdot L^*}{k_L}. \quad (18)$$

From Eqs. (17) and (18), film Nusselt number for laminar film can be expressed as

$$Nu_L = \frac{L^*}{\delta} = \frac{1}{\delta^*}. \quad (19)$$

Above theoretical Nusselt number is based on the assumption of smooth liquid film. However, actual film surface shows waviness and rippling. The waviness and rippling enhance the heat transfer in the film. Also, turbulent film transition can occur at very low film Reynolds number for high interfacial shear condition. Hughmark [18] developed model for liquid film thickness based on many experimental data. The model showed that the dimensionless film thickness for very small film Reynolds number is continuously matching with one for very high film Reynolds number, i.e., turbulent film. It means that transition to turbulent film can occur at very small film Reynolds number. To take into account the heat transfer enhancement due to film wave and turbulent effects, McAdams [19] modified Eq. (19) by the multiplication factor of 1.2.

Blangetti et al. [20] developed the empirical film model applicable to a wide range of film Reynolds number as

$$Nu_L = (Nu_{L,lam}^4 + Nu_{L,tur}^4)^{1/4}. \quad (20)$$

Laminar film Nusselt number ($Nu_{L,lam}$) is the theoretical value as shown in Eq. (19). For turbulent film Nusselt number ($Nu_{L,tur}$) they suggested the following empirical equation:

$$Nu_{L,tur} = c_1 \cdot Re_L^{c_2} \cdot Pr_L^{c_3} \cdot (1 + c_4 \cdot (\tau_I^*)^{c_5}), \quad (21)$$

where, c_1–c_5 are constant depending on the dimensionless shear stress, τ_I^*.

To take into account the effects of film waviness and transition regime between laminar and turbulent film, Blangetti model in Eq. (20) is used for the present analysis. The heat transfer in the film region is coupled with the momentum, energy, and mass transfer in the gas region through the parameters such as film thickness, interfacial shear stress, and film flow rate. The transport phenomena in the gas region are discussed in the next section. Film properties are evaluated at the film temperature, which is the arithmetic mean of the inside wall temperature and interface temperature.

3.3. Momentum, heat and mass transfer in gas region

The momentum, heat and mass transfer and the effects of suction in the gas region are discussed in this section. Since the condensation can be regarded as a kind of wall suction, the results of the transpiration effects could be applied to the condensation problem. Characteristics of the momentum, heat and mass transfer are affected dramatically for the transpiration boundary layer such as suction or blowing at the wall. For arbitrary variation of the suction or blowing velocity, Couette flow analysis has been used [21]. Although the derivation procedure in Couette flow analysis is based on constant suction or blowing velocity for the external boundary layer, it can be used for arbitrary changing suction or blowing velocity by assuming that the suction or blowing velocity is constant at each small domain of calculation. Also, it is assumed to be valid for internal boundary layer such as a pipe flow. The effect of transpiration was formulated by the ratio of the dimensionless transport quantity with transpiration to one without transpiration as a function of blowing parameter. The dimensionless quantities for momentum, heat and mass transfer are friction coefficient (f), heat transfer Stanton number (St) and mass transfer Stanton number (St_m), respectively. These quantities and the corresponding blowing parameters are defined in Table 2. Subscript 0 in Table 2 represents the quantity without transpiration. It should be noted that the blowing parameter is negative for suction and positive for blowing and suction enhances the momentum, heat and mass transfer, i.e., condensation is characterized with the enhanced transport mechanism at the interface due to the surface suction effect.

Now, we need to find the correlations at no transpiration boundary. A large number of the correlation for momentum, heat and mass transfer without transpiration has been developed in pipe flow [21,22]. A proper choice of the transport correlations is crucial for the heat and mass analogy model. To choose most appropriate correlations, the boundary layer model developed by authors [15] is used. In the boundary layer model, two sets of governing equations for liquid film and vapor–gas mixture regions were numerically solved and the model was validated with various available condensation data. From the analysis results, the best fitting correlations for momentum, heat and mass transfer are selected and summarized in Table 2. A detailed procedure can be found in [16].

For the momentum transfer, interfacial friction factor is determined as follows: First, the interfacial friction factor for no suction condition (f_0) is estimated using the gas

Table 2
Correlations, transpiration effects and blowing parameters [21,22]

Transport mode	Correlations		Transpiration effect	Blowing parameter
	Laminar flow	Turbulent flow		
Momentum, f_0	$f_0 = \frac{16}{Re_d}$	$f_0 = 0.079 \cdot Re_d^{-0.25}$	$\frac{f/2}{(f/2)_0} = \frac{b_f}{\exp(b_f) - 1}$	$b_f = \frac{m''/G_\infty}{(f/2)_0}$
Heat, St_0 or Nu_0	$Nu_0 = 4.364$	$Nu_0 = 0.022 \cdot Re_d^{0.8} \cdot Pr^{0.5}$	$\frac{St}{St_0} = \frac{b_h}{\exp(b_h) - 1}$	$b_h = \frac{m''/G_\infty}{St_0}$
Mass, St_{m0} or Sh_0	$Sh_0 = 4.364$	$Sh_0 = 0.022 \cdot Re_d^{0.8} \cdot Sc^{0.5}$	$\frac{St_m}{St_{m0}} = \frac{g_m}{g_{m0}} = \frac{b_m}{\exp(b_m) - 1}$	$b_m = \frac{m''/G_\infty}{St_{m0}}$

mixture Reynolds number. Then, the blowing parameter for momentum transfer (b_f) is calculated. In the actual analysis, the mass flux terms for suction/blowing (m'') and free stream ($G_\infty = \rho_\infty u_\infty$) in the blowing parameters are modified with condensation mass flux (m''_c) and bulk mixture mass flux (ρu_{avg}) for the previous iteration, respectively. Finally, the interfacial friction factor with suction effect (f) can be determined from the momentum transfer blowing parameter (b_f) and the interfacial friction factor for no suction condition (f_0) using the expression in Table 2. Interfacial shear stress is calculated using the following definition of the interfacial friction factor:

$$f \equiv \frac{\tau_I}{\rho \cdot (u_{avg} - u_{L,avg})^2/2}. \tag{22}$$

Here, it should be noted that the velocity component in the above equation must be a relative velocity between the gas and film regions.

For the sensible heat transfer, sensible heat transfer Nusselt number (Nu_{sen}) is determined by the similar procedure using the heat transfer blowing parameter (b_h) and the heat transfer Stanton number for no suction condition (St_0). The sensible heat transfer coefficient (h_{sen}) is calculated using the following definition:

$$Nu_{sen} \equiv \frac{h_{sen} \cdot d}{k}. \tag{23}$$

For the mass transfer, mass transfer Sherwood number (Sh) is also determined using the mass transfer blowing parameter (b_m) and the mass transfer Stanton number for no suction condition (St_{m0}). Mass transfer conductance (g_m) extracted from the mass transfer Sherwood number can be related with the diffusive mass flux of NC gas as

$$g_m \equiv \frac{j_{v,I}}{W_{v,I} - W_{v,b}} = \frac{j_{g,I}}{W_{g,I} - W_{g,b}} = \frac{j_I}{W_I - W_b}. \tag{24}$$

In the above equation, the relationships of $j_v + j_g = 0$, $W_v + W_g = 1$ are used and subscript g for j_g and W_g, is omitted for simplification. Since the radial velocity of the NC gas is zero at the interface, the diffusive mass flux of NC gas at the interface (j_I) can be expressed as follows using the definition of the NC gas diffusive mass flux ($j_g \equiv \rho_g(v_g - v)$):

$$j_I = -W_I m''_c. \tag{25}$$

Combining Eqs. (24) and (25), the condensation mass flux can be determined.

The relationship between vapor partial pressure and NC gas mass fraction at interface or bulk is expressed from Gibbs–Dalton ideal gas mixture equation:

$$\frac{p_v}{p_{TOT}} = \frac{1 - W}{1 - W(1 - M_v/M_g)}. \tag{26}$$

Mixture viscosity, mixture thermal conductivity and mass diffusion constant are calculated using the theory of the gas transport properties [23]. Specific heat capacity for the mixture is simply calculated by mass fraction weighted average:

$$C_p = W \cdot C_{pg} + (1 - W) \cdot C_{pv}. \tag{27}$$

3.4. Calculation procedure

The calculation procedures are summarized as follows:

(1) Specify inlet and boundary conditions.
(2) Initialize the variables and parameters for next axial node.
(3) Assume interface temperature, condensation mass flux, interface shear and calculate relevant parameters.
(4) Calculate film thickness from film mass balance.
(5) Calculate film Nusselt number.
(6) Calculate blowing parameters.
(7) Calculate interfacial friction factor, heat transfer Nusselt number and mass transfer Sherwood number.
(8) Calculate total condensation heat transfer coefficient.
(9) Calculate total heat flux, condensation mass flux and interfacial shear.
(10) If interface temperature, condensation mass flux, total heat flux and interface shear converge, go to Step 11. If not, update interface temperature and go to Step 4 for the next iteration.
(11) Go to Step 2 for the next axial node.

3.5. Analysis results

The heat and mass analogy model is run for the present experiment conditions. Fig. 7 compares the tube average condensation HTC for various conditions with inlet NC gas mass fraction. Fig. 7(a) shows the effects of pressure for a given inlet steam flow rate of 3.8 g/s and Fig. 7(b) shows the effects of inlet steam flow rate for a given system pressure of 0.34 MPa. The analogy model predicts very well the general trend of experimental data: The condensation HTC decreases with the increase of the NC gas fraction and system pressure and it increases with the increase of inlet steam flow rate. For low inlet NC gas mass fraction cases, the model underestimates the heat transfer coefficient. This trend is mainly due to the heat transfer enhancement from the film waviness. A large amount of condensation due to low inlet NC gas mass fraction results in higher film Reynolds number. As the film Reynolds number increases, the effect of the film waviness acts more role in the heat transfer mechanism. The wave itself increases the condensation surface area and it enhances the thermal mixing in the liquid film. Fig. 8 compares the calculated and the measured average condensation HTC for the present experimental data.

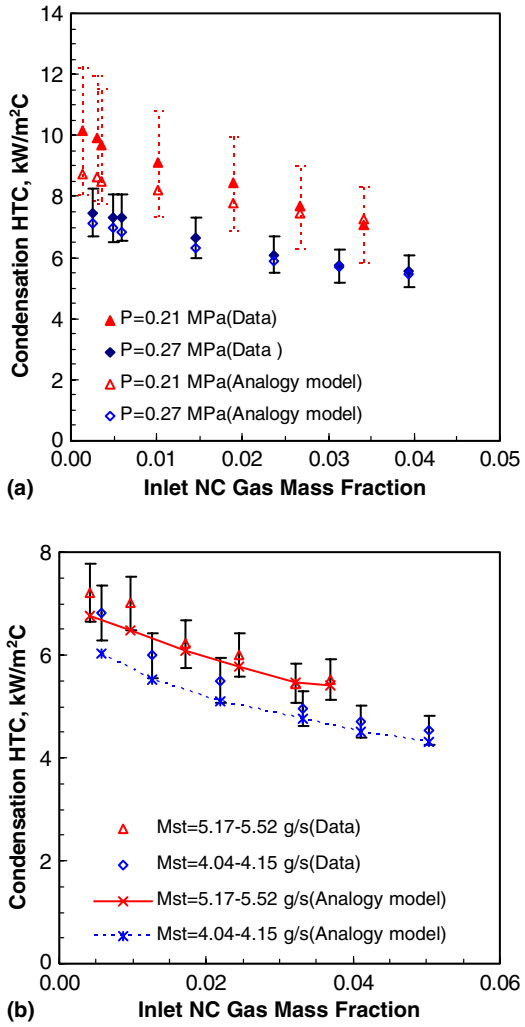

Fig. 7. Comparison of average condensation HTC with respect to inlet NC gas mass fraction: (a) inlet steam flow = 3.8 g/s and (b) system pressure = 0.34 MPa.

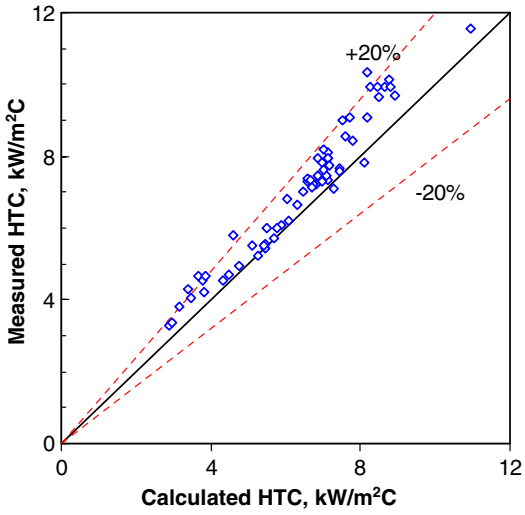

Fig. 8. Comparison of average condensation HTC with analogy model.

Developed heat and mass analogy model is also tested for Kuhn's [5] experimental conditions. Kuhn performed the condensation experiment with secondary jacket cooling method with 47.5 mm ID, 2.1 m length condenser tube. He reported the local condensation HTC up to 1.5 m from the tube inlet. The experiment cases used in this paper is the run number 212 and 2112: nominal inlet steam flow rate of 50 kg/h, system pressure of 0.41 MPa. Inlet air mass fractions for the run number 212 and 2112 are 2% and 34%, respectively. The comparison of the local condensation HTC between data, the present heat and mass analogy model, and the boundary layer model [15] is presented in Fig. 9. The relative error of the local condensation HTC was reported as 18.7% [5] and the error bars are drawn based on this value. Both models predict very well the data. For low inlet NC gas fraction (2%) case, both models slightly underestimate the local condensation HTC near the end of tube (1.5 m from inlet). This trend is also due to the film waviness, explained previously. The film Reynolds numbers at 1.5 m from inlet are around 1100 for low inlet NC gas

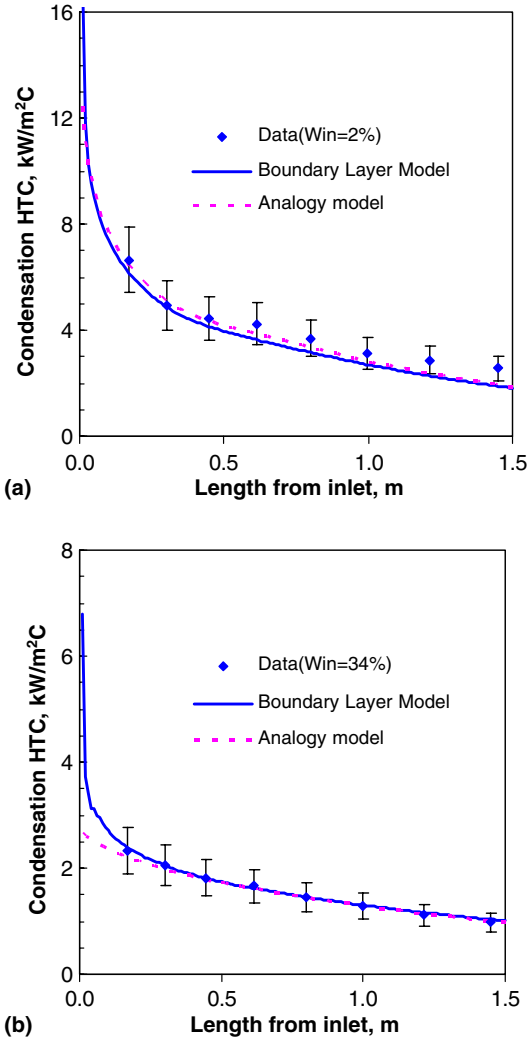

Fig. 9. Comparison of local condensation HTC for Kuhn's experiment. Inlet NC gas mass fraction: (a) 2% and (b) 34%.

fraction (2%) case and around 500 for high fraction (34%) case. The results of the analogy model are almost identical to those of the boundary layer model except for the tube inlet region. As discussed in Section 3.3, the momentum, heat and mass transfer correlations applied in the analogy model are validated with the boundary layer model. This is the reason why the analogy model results are very similar to the boundary layer analysis results. Also, the discrepancy between two models at tube inlet region is originated from the fact that the correlations for the momentum, heat and mass transport used in the analogy model is based on the fully developed flow condition.

4. Conclusion

Experimental and theoretical investigation was conducted for a vertical in-tube condensation system with the presence of the noncondensable gas. Condensation experiments were performed with a vertical tube condenser, which is submerged in the secondary water pool where the condensation heat transferred from the tube is removed by the boiling. This type of the condenser has been designed in the PCCS of the SBWR. A PCCS condenser tube with half-length and half-diameter scale was used to obtain the condensation heat transfer coefficient. The condensation heat transfer coefficient and heat transfer rate decrease with the noncondensable gas. The condensation heat transfer rate is enhanced by increasing the inlet steam flow rate and the system pressure. The condensation heat transfer coefficient increases with the inlet steam flow rate, however, decreases with the system pressure. The present experimental data provide a new database for the in-tube steam condensation with noncondensable gas submerged in water pool for the PCCS operating conditions.

A heat and mass analogy model is developed to predict the filmwise condensation with the noncondensable gas. This model uses the momentum, heat, and mass transport correlations selected from the general relationships, which have the strong theoretical background and the less empiricism. The effects of the surface suction at the condensation interface were taken into account in the correlations. The analysis results of the model were compared with the average condensation heat transfer coefficient data in the present experiment and the local condensation heat transfer coefficient data in Kuhn's experiment [5] and the agreement was satisfactory. For a large film Reynolds number region, the model slightly underestimates the condensation heat transfer coefficient due to the heat transfer enhancement by the film waviness. A proper consideration of the wavy film into the model will improve the prediction capability of the model.

Acknowledgements

This work was supported by US Department of Energy under Nuclear Energy Education Research (NEER) research grant with award number DE-00ID13928 for a project entitled: Analytical and Experimental Study of the Effects of Non-Condensable in a Passive Condenser System for the Advanced Boiling Water Reactor.

References

[1] J.G. Collier, Convective Boiling and Condensation, second ed., McGraw-Hill, New York, 1981.
[2] GE Nuclear Energy, SBWR standard safety analysis report, 25A5113, Rev A, 1982.
[3] K.M. Vierow, Behavior of steam–air systems condensing in concurrent vertical downflow, M.S. Thesis, University of California at Berkeley, 1990.
[4] M. Siddique, The effects of noncondensable gases on steam condensation under forced convection conditions, Ph.D. Thesis, Massachusetts Institute of Technology, 1992.
[5] S.Z. Kuhn, Investigation of heat transfer from condensing steam–gas mixtures and turbulent films flowing downward inside a vertical tube, Ph.D. Thesis, University of California at Berkeley, 1995.
[6] H.S. Park, H.C. No, A condensation experiment in the presence of noncondensables in a vertical tube of a passive containment cooling system and its assessment with RELAP5/MOD3.2, Nucl. Technol. 127 (1999) 160–169.
[7] A.P. Colburn, O.A. Hougen, Design of cooler condensers for mixture of vapors with noncondensing gases, Ind. Eng. Chem. 26 (1934) 1178–1182.
[8] C.Y. Wang, C.J. Tu, Effects of noncondensible gas on laminar film condensation in a vertical tube, Int. J. Heat Mass Transfer 31 (1988) 2339–2345.
[9] M. Siddique, M.W. Golay, M.S. Kazimi, Theoretical modeling of forced convection condensation of steam in a vertical tube in the presence of a noncondensable gas, Nucl. Technol. 106 (1994) 202–214.
[10] S.M. Ghiaasiaan, B.K. Kamboj, S.I. Abdel-Khalik, Two fluid modeling of condensation in the presence of noncondensible gas in two phase channel flows, Nucl. Sci. Eng. 119 (1995) 1–17.
[11] J.L. Munoz-Cobo, L. Herranz, J. Sancho, I. Tkachenko, G. Verdu, Turbulent vapor condensation with noncondensable gases in vertical tubes, Int. J. Heat Mass Transfer 39 (1996) 3249–3260.
[12] A. Dehbi, S. Guentay, A model for the performance of a vertical tube condenser in the presence of noncondensable gases, Nucl. Eng. Des. 177 (1997) 41–52.
[13] S.Z. Kuhn, V.E. Schrock, P.F. Peterson, An investigation of condensation from steam–gas mixtures flowing downward inside a vertical tube, Nucl. Eng. Des. 177 (1997) 53–69.
[14] H.C. No, H.S. Park, Non-iterative condensation modeling for steam condensation with non-condensable gas in a vertical tube, Int. J. Heat Mass Transfer 45 (2002) 845–854.
[15] S. Oh, S.T. Revankar, Boundary layer analysis for steam condensation in a vertical tube with noncondensable gases, Int. J. Heat Exchanger 6 (2005) 93–124.
[16] S. Oh, Experimental and analytical study of the effects of noncondensable gas in a passive condenser system, Ph.D. Thesis, Purdue University, 2004.
[17] S. Oh, S.T. Revankar, Effect of noncondensable gas in a vertical tube condenser, Nucl. Eng. Des. 235 (2005) 1699–1712.
[18] G.A. Hughmark, Film thickness, entrainment, and pressure drop in upward annular and dispersed flow, Amer. Inst. Chem. Eng. J. 19 (1973) 1062–1065.
[19] W.H. McAdams, Heat Transmission, third ed., McGraw-Hill, New York, 1954.
[20] F. Blangetti, R. Krebs, E.U. Schlunder, Condensation in vertical tubes—experimental results and modeling, Chem. Eng. Fundam. 1 (1982) 20–63.
[21] W.M. Kays, W.M.E. Kays, Convective Heat and Mass Transfer, third ed., McGraw-Hill, New York, 1993.
[22] A.H.P. Skelland, Diffusional Mass Transfer, John Wiley & Sons, New York, 1974.
[23] B.R. Bird, W.E. Stewart, E.N. Lightfoot, Transport Phenomena, second ed., John Wiley & Sons, Inc, New York, 2002.